A syntrophic interdomain biofilm composed of *Methanobacterium cahuitense* and *Desulfomicrobium aggregans* reveals novel microbial interaction strategies

Linda Dengler[1*], Laura Kuschmierz[2], Bernd Daller[1,3#], Andreas Klingl[4], Julia Meier[1], Martina Althammer[5], Annett Bellack[1], Raimund Tenhaken[5], Winfried Hausner[1], Wolfram Gronwald[3], Claudia Bogner[3], Sarah Coffinet[6,7#], Kai-Uwe Hinrichs[6], Bettina Siebers[2], Reinhard Rachel[8], Dina Grohmann[1*], Harald Huber[1]

Affiliation

[1] Institute of Microbiology and Archaea Centre, University of Regensburg, Regensburg, Germany

[2] Molecular Enzyme Technology and Biochemistry, Environmental Microbiology and Biotechnology, and Centre for Water and Environmental Research, University of Duisburg-Essen, Essen, Germany

[3] Institute of Functional Genomics, University of Regensburg, Regensburg, Germany

[4] Plant Development and Electron Microscopy, Biocenter LMU Munich, Planegg-Martinsried, Germany

[5] Molecular Plant Physiology, University of Salzburg, Salzburg, Austria

[6] MARUM – Center for Marine Environmental Sciences and Department of Geosciences, University of Bremen, Bremen, Germany

[7] UMR ECOBIO, Université de Rennes, CNRS, Rennes, France

[8] Center for Electron Microscopy, University of Regensburg, Regensburg, Germany

current address

[3] Institute of Functional Genomics, University of Regensburg, Regensburg, Germany

[7] UMR ECOBIO, Université de Rennes, CNRS, Rennes, France

* corresponding author

Linda Dengler, linda.dengler@ur.de

Dina Grohmann, dina.grohmann@ur.de

ORCiD information

Linda Dengler: https://orcid.org/0000-0003-1856-2100

Andreas Klingl: https://orcid.org/0000-0001-8414-8317

Annett Bellack: https://orcid.org/0000-0001-9771-0348

Raimund Tenhaken: https://orcid.org/0000-0002-6764-4826

Winfried Hausner: https://orcid.org/0000-0002-4382-7468

Wolfram Gronwald: https://orcid.org/0000-0003-3646-0060

Sarah Coffinet: https://orcid.org/0000-0002-6753-9460

Kai-Uwe Hinrichs: https://orcid.org/0000-0002-0739-9291

Bettina Siebers: https://orcid.org/0000-0002-9905-541X

Reinhard Rachel: https://orcid.org/0000-0001-6367-1221

Dina Grohmann: https://orcid.org/0000-0002-0570-2517

Harald Huber: https://orcid.org/0000-0003-4251-6091

Competing Interests Statement

47 This work was supported by funds provided by the University of Regensburg to D.G. The authors
48 declare no competing interests. L.D., D.G., and H.H. are co-founders of Microbify GmbH,
49 Germany. However, there are no commercial interests by the company, nor is any financial
50 support granted by Microbify GmbH.

Abstract

Sulfate-reducing bacteria (SRB) can interact with other microorganisms to form inter-species communities including methanogenic archaea. However, the nature of these communities is complex, and the diversity of syntrophic options remains to be fully elucidated. In this study, we utilize a biofilm community formed by the methanogen *Methanobacterium cahuitense* and the SRB *Desulfomicrobium aggregans* to elucidate the functional interactions, spatial cell distribution, cellular properties, syntrophic exchange of metabolites, and composition of the extracellular polymeric substance (EPS) of this interdomain biofilm. Notably, we compared the natural consortium isolated from an oil well with an artificial consortium comprised of the previously isolated individual organisms.

We show that *D. aggregans* cells form clusters even in the absence of the methanogen and produce a significant quantity of the EPS establishing a biofilm matrix capable of accommodating *M. cahuitense* cells. Electron tomography revealed cellular substructures like an enlarged periplasm and an undulating cytoplasmic membrane in *D. aggregans*. Lipidomic analyses identified novel archaeal lipids and, for the first time, a rare deoxyhexose archaeol in *Methanobacterium.* A bacterial hydroxylated lipid was found in the co-culture only, suggesting that the membrane composition is finely tuned to the biofilm state. Metabolomic analysis showed that the SRB produces formate, while *M. cahuitense* generates propionate indicating the possibility for novel metabolite exchange pathways that reinforce the syntrophic interaction between SRBs and methanogens. The findings of this study thereby contribute to our understanding of how SRBs and methanogens benefit from a mutualistic lifestyle within a specific ecological niche.

Introduction

Biofilms are impressively sophisticated, three-dimensional structures, that are created, modified, and dismantled by microorganisms. Their formation typically starts with cell adhesion to a surface which then activates second messengers like cyclic di-guanosinemonophosphate that play a role in intra- and intercellular communication. In Gram-negative bacteria, quorum sensing plays a role in the recruitment of cells for biofilm growth [1]. Archaeal biofilm formation was comprehensively studied in members of the *Sulfolobales* [2–4]. Biofilms formed by methanogens play a crucial role in microbiologically influenced corrosion in biogas, oil, and natural gas infrastructure, however, the exact mechanisms are still poorly understood [5].

The extracellular polymeric substance (EPS) embodies the biofilm scaffold and was vividly described as the "house of biofilm cells" [6]. It comprises a diverse matrix of polysaccharides, (glyco-)proteins, nucleic acids, metabolites, siderophores, and metals, among others [7]. Its main component, however, is water. It is absorbed by the polymers, displays an inseparable part of functional channels, and contributes to up to 90% of the total biofilm wet weight [8]. The EPS functions as a protective barrier against environmental stressors like antibiotics, it eases cell-cell communication [9], and enables positioning and attachment in the vicinity of valuable nutrient sources. These properties are of great importance in natural habitats, where environmental conditions can change drastically in an unpredicted manner and additional stressors like harmful chemicals or viruses may compromise the microbes.

Until today, several complex, syntrophic archaeal and interdomain liaisons were discovered: SM1 Euryarchaeon and *Thiotrix* sp. thrive in close proximity to one another embedded in a string-of-pearl structure [10], while *Ignicoccus hospitalis* and *Nanoarchaeum equitans* were shown to be able to establish a cell-cell-linkage for direct metabolic interactions [11,12]. Recently, cryotomography revealed that the DPANN *Microcaldus variisymbioticus* can interact with its host, *Metallosphaera javensis*, by establishing proteinaceous cell-to-cell nanotubes [13]. Tangible

syntrophic strategies include increased conjugation rates in biofilms compared to planktonic cells [14], direct interspecies electron transfer (DIET) [15], and nutrient exchange [16].

In this study, the unique co-culture of the methanogenic archaeon *Methanobacterium cahuitense* and the sulfate-reducing bacterium *Desulfomicrobium aggregans* were characterized. These organisms form a biofilm in an anoxic, water-filled pond of an ancient oil well in Costa Rica [17]. Previous studies have shown that the sulfate reducer forms dense biofilm aggregates when inoculated alone or together with the methanogen. Both organisms are exceptionally intertwined, e.g. cross-cultivation experiments with their closest phylogenetic relatives *Methanobacterium subterraneum* and *Desulfomicrobium baculatum* failed [17]. In sulfate-rich environments, sulfate reducers typically outcompete methanogens due to a higher substrate affinity towards the valuable electron donor H_2 [18,19]. In contrast to methanogens that possess a rather limited substrate spectrum, sulfate reducers benefit from their metabolic flexibility: they utilize several electron acceptors like sulfate, sulfite, thiosulfate, or elemental sulfur, while a variety of organic acids can serve as electron donors; in addition, they are able to thrive fermentatively [20]. In multispecies anaerobic biofilms, competition and co-existence of methanogens and sulfate-reducing bacteria seemingly go hand-in-hand. With increased sulfate levels, the sulfate-reducing populations prosper, and simultaneously, methanogenic cell numbers decrease until a steady-state-level is acquired [21]. Metabolic conjunction was also reported for a number of marine methanogens that produced minor amounts of hydrogen and therewith enabled co-existence with sulfate reducers [22].

In this study, we employed multiple -omics and imaging approaches and provide novel insights into cell-cell interactions and a syntrophic relationship in this inter-species biofilm formed by *Methanobacterium cahuitense* and *Desulfomicrobium aggregans*, which is unique due to the co-existence of methanogens and sulfate reducers under hydrogen and sulfate-rich conditions. The

analyses show that the interactions of both microbes are reflected in adaptive alterations in cell structure (tomography) and biochemical composition (e.g. lipids, EPS), and also in the likely exchange of small organic metabolites, notably formate and propionate.

Material and Methods

All experiments in this study refer to the pure cultures of *Methanobacterium cahuitense* (M) and *Desulfomicrobium aggregans* (S), the original consortium of them isolated from the environment (K), and an artificial co-culture comprised of both pure cultures (Ka).

All cultures were cultivated in MS-Sulf medium [17] supplemented with 0.1% acetate (w/v) under a H_2/CO_2 (80:20 v/v, 300 kPa) atmosphere at 37°C with shaking (70 rpm).

Electron Microscopy and Electron Tomography

The structural survey of the biofilm was the foundation for understanding the interdomain interactions. To preserve the biofilm and cell structure in a near-to-natural state for electron microscopy, cryo-techniques were used for preparation [23]. For high-pressure freezing, 1.4 µl of biofilm-aggregates from an exponentially grown consortium culture were carefully taken up with a pipet tip, loaded into Aluminium planchettes, and cooled at a pressure of 210 MPa (HPM100 high-pressure freezer; Leica Microsystems, Germany). Freeze substitution was done using acetone containing 2% (w/v) OsO_4 and 0.2% uranyl acetate (EM AFS2 freeze substitution unit; Leica Microsystems, Germany) following the protocol: −90°C for 20 h, heating to −60°C within 3 h, −60°C for 8 h, heating to −30°C within 3 h, −30°C for 8 h and finally heating to 0°C within 3 h. After washing cells two times with pure acetone at 0°C, cells were embedded in Spurr's resin/acetone (1 + 1) for 1 h, and resin/acetone (2 + 1) for 2 h, and infiltrated in 100% resin overnight. Final polymerization was carried out at 63°C for 12 h. Thin sections of 80 – 500 nm were cut with an ultramicrotome (Ultracut E; Reichert-Jung, Leica Microsystems Germany) and collected on Collodium-coated 75 square mesh Cu grids (Science Services, Germany). Ultrathin sections (80 nm) were post-stained for 2 min with lead citrate. For electron tomography, sections were not post-stained; tomography datasets were recorded from nominally 500 nm thick sections with a tilting range from +66° to -66° on a transmission electron microscope operated in

scanning transmission electron microscopy (STEM) mode (JEM-2100F; JEOL, Germany) using a bright-field STEM detector and, for searching, an F416 CMOS camera (TVIPS, Gilching, Germany) using SerialEM (v. 3.8) [24,25]. 3D reconstruction and image segmentation were performed using IMOD (v. 4.12) [26].

Light Microscopy, Modified DOPE-FISH and Confocal Laser Scanning Microscopy (CLSM)

Due to the presence of electron-dense, intracellular structures in both organisms, Nile red staining was performed to test for the presence of intracellular lipid storages, in particular polyhydroxyalkanoates (PHA) and polyhydroxybutyrates (PHB) [27,28]. To this end, a well-grown consortium culture was incubated with Nile red dissolved in DMSO at a final concentration of 0.5 µg ml^{-1} for 10 min and surveyed on an Olympus BX60 (excitation filter HQ 546/12, dichromatic mirror Q 560 LP, suppression filter HQ 585/40) [28].

As standard FISH (fluorescence in situ hybridization) techniques failed due to poor fluorescence signal in the dense biofilm, a combination of DOPE-FISH (double labeling of oligonucleotide probes) [29,30] with CARD-FISH (catalyzed reporter deposition) hybridization buffer was applied [31]. Here, Arch915 [32] and EUB388 [33] were used as archaeal and bacterial FISH probes doubly-labeled with either Oregon Green or Cy5, respectively. Cy5-labeled NON-EUB was used as negative control [34]. Exponentially grown cultures were fixed in 96% EtOH, air-dried on microscope slides, and embedded in 0.1% agarose. Permeabilization was achieved by treatment with lysozyme (10 mg ml^{-1}) and achromopeptidase (60 U ml^{-1}) (Sigma-Aldrich) using 0.15% H_2O_2 in phosphate-buffered saline (PBS; pH 7.3) [35].

Hybridization, washing, and tyramide signal amplification were carried out according to standard CARD-FISH protocols [36] under 35% formamide with overnight hybridization at 46°C. Samples

were imaged with a DMi 8 confocal microscope at 63x/1.40 oil and processed with Leica Application Suite X software package (Leica Microsystems, Germany).

Exopolysaccharide Staining with Fluorescently Labeled Lectins

To detect and visualize the type and distribution of extracellular sugars within the EPS, fluorophore-labeled lectins were applied to S, M and K-cultures, with concanavalin A (ConA) binding to α-mannopyranosyl and α-glucopyranosyl residues, and isolectin GS-IB4 (IB4) targeting α-D-galactosyl residues. 20 µl of ConA-FITC (fluorescein isothiocyanate dextran) solution (10 µg ml^{-1}) and 8 µl of IB4-Alexa Fluor™ 594 solution (8 µg ml^{-1}) were used for lectin staining as described [37]. To counterstain the cells, 0.2 % (w/v) DAPI (4,6-diamidino-2-phenylindole) solution [38] with 0.01 % (w/v) sodium dodecyl sulfate (SDS) was applied for 3 min. To avoid detachment during rinsing, clean microscope slides were coated with gelatine solution (0.1% (w/v) gelatine, 0.01 % (w/v) $KCr(SO_4)_2 \times 12\ H_2O$) prior to use [39]. Samples were then applied onto the slides, embedded with CitiFluor™ AF1 (Citifluor Ltd., UK), and imaged using an inverted TCS SP8 SMD confocal laser scanning microscope with a 63x/1.40 oil immersion objective (Leica Microsystems, Wetzlar, Germany). Images were processed with ImageJ (v. 1.54) [40].

EPS Extraction, Compound Quantification and High-Performance Liquid Chromatography (HPAEC-PAD)

To quantify the extracellular proteins, sugars, and eDNA (extracellular DNA), EPS was extracted. As EPS extraction from dense cell aggregates is uniquely challenging, different extraction methods were tested (data not shown). This initial screening included extractions with crown ether, EDTA, and different amounts of cation exchange resin (CER) as previously described [41]. The CER method was identified as the best option, enabling the isolation of sufficient amounts

196 of EPS, while preserving cell integrity. EPS isolation started with 0.2 g of cell mass (wet weight)
197 which were treated with 2 g of CER (Dowex® Marathon® C sodium form, Sigma-Aldrich) in
198 10 ml phosphate buffer (2 mM Na_3PO_4, 4 mM NaH_2PO_4, 9 mM NaCl, 1 mM KCl, pH 7.0).
199 Sample triplicates were then vortexed at maximum speed for 10 min and treated by ultrasound
200 using a Sonorex Super 10P device (BANDELIN electronic, Germany) at 80% power for 3 min
201 each. This process was repeated six times until the biofilm was fully disintegrated. Cell integrity
202 was microscopically controlled after each cycle by phase contrast light microscopy and
203 subsequent sample processing was performed according to Jachlewski et al. [41]. Finally, the
204 biofilm suspension (BF), the total extracellular material (TEM) with low and high molecular
205 weight compounds, as well as the EPS fraction containing molecules larger than 3.5 kDa were
206 further analyzed. Protein, carbohydrates, and eDNA concentrations were measured in technical
207 triplicates using a modified Lowry assay [42], Dubois assay [43], and the Qubit™ dsDNA HS
208 assay kit (Thermo Fisher Scientific), respectively [44].
209 Sugars were additionally analyzed by High-Performance Liquid Chromatography (HPLC) based
210 on a previously described method [45]. HPLC separations were performed on a high-performance
211 anion-exchange chromatography with pulsed amperometric detection (HPAEC-PAD) system
212 (Model ICS3000; Dionex) consisting of an ICS3000 Single Pump, ICS3000 electrochemical
213 detector and a Dionex AS autosampler. Columns in use were a Dionex CarboPac PA20 column
214 (150 x 3 mm i.d., 6.5 µm particle size) with a PA20 guard column (30 x 3 mm i.d., 6.5 µm particle
215 size). The mobile phase consisted of (A) 200 mM NaOH, (B) 15 mM NaOH, (C) 50 mM NaOH,
216 500 mM NaAc, and (D) 1 mM NaOH. EPS composition measurements were conducted on the
217 PA20 CarboPac column. All sugars except xylose and mannose were analyzed by the following
218 method: it started with an equilibration run at -13 min with 100% solvent A. Starting conditions
219 were held for 5 min until -8 min. From -8 to -7 min 100% of solvent B was reached and held until
220 8 min. Here a gradient of 50% B and 30% C was established from 8 to 8.2 min. From 8.2 to 13

min the gradient of C changed to 50% and B remained at 50%. This gradient was held until the end at 22 min. A post-run with 100% B followed for 0.1 min.

Xylose and mannose were measured on the same column but with a different gradient. The method started with a pre-flow pipe at -20 min with 100% solvent A. Starting conditions were held for 6 min until -14 min. From min -14 to -13 min a gradient setting of 10% solvent B and 90% D was established within 1 min. This gradient was held until the end in 25 min.

Metabolite Extraction and Nuclear Magnetic Resonance Spectroscopy (NMR)

To gather information on the metabolic properties, metabolites were analyzed in triplicates using nuclear magnetic resonance spectroscopy (NMR). Cells were collected from 7 ml culture by centrifugation (3,000×g, 30 min, 4°C) and the supernatant was stored at –20°C upon further usage. The pellet was washed in 1x PBS thrice and further processed by a 1 h achromopeptidase treatment (125 U ml^{-1}) at 37°C followed by sonication at 80% amplitude for 1 min using Bandelin Sonopuls HD 2070 (BANDELIN electronic, Germany). Incubation at 37°C and sonication were repeated twice until phase contrast microscopy confirmed the complete lysis of *Methanobacterium* cells. The pellet was resuspended in 600 µl MeOH (80% v/v) and stored at –80°C.

To extract intracellular hydrophilic metabolites, 2 mM nicotinic acid and 1.6 ml MeOH were added. This mixture was frozen at –80°C overnight and centrifuged at 10,000×g for 5 min at 4°C. The supernatant was transferred into an amber glass vial, while the pellet was washed twice with 200 µl MeOH (80% v/v), pelleted at 10,000×g for 5 min, and finally at 12,000×g. All supernatants were merged and evaporated, while the intracellular extract was diluted in 400 µl H_2O and with 200 µl of 0.1 M phosphate buffer (0.1 M K_2HPO_4, 0.1 M KH_2PO_4, 0.39 mM boric acid; pH 7.4), and 50 µl of 0.75% (w) 3 trimethylsilyl 2,2,3,3 tetradeuteropropionate (TSP) dissolved in D_2O as internal standard (Sigma-Aldrich). For the analysis of extracellular metabolites, 400 µl of

supernatant was mixed with buffer and D_2O as described above. NMR measurements were performed on a 600 MHz Avance III spectrometer (Bruker BioSpin, Germany). For every specimen, 1D ^1H spectra were collected following established protocols [46]. In short, 1D NOESY (nuclear overhauser enhancement spectroscopy) pulse sequence with presaturation during relaxation and mixing time with additional spoil gradients for water suppression was used. 128 scans were collected into 64 k data points over a 20 ppm spectral width using a relaxation delay of 4 s, an acquisition time of 2.66 s, and a mixing time of 0.01 s.

From the obtained NMR spectra, absolute metabolite concentrations were determined with the Chenomx software (v. 9.02; Chenomx Inc., Canada). For statistical data analysis of NMR fingerprinting data, bucket tables were generated from 1D ^1H NMR spectra for statistical data analysis using AMIX 3.9.13 (Bruker BioSpin, Germany). An optimized bucket size of 0.01 ppm was applied to compensate for variations in NMR signal positions. Further analysis was performed using R (v. 4.4.1) [47]. The data was normalized with variance stabilizing normalization (VSN) [48]. Buckets containing water signals or artificially introduced agents were excluded from the analysis. Subsequently, Principal Component Analysis (PCA) was carried out.

Lipid Extraction and Ultra-High Performance Liquid Chromatography-Mass Spectrometry (UHPLC-MS) Analysis

For the extraction of lipids, a modified method based on the method by Bligh & Dyer [49] was used as described [50]. Lipids were analyzed using UHPLC-MS methods based on hydrophilic interaction chromatography (HILIC) and long reversed phase (RP) chromatography. For intact polar lipid (IPL) separation, a Waters Acquity UPLC BEH Amide column (150 mm × 2.1 mm, particle size 1.7 µm, Waters Corporation, Germany) was used with the HILIC method described by Wörmer et al. [51]. Compounds with lower polarity such as glycerol dialkyl glycerol tetraethers (GDGT) were analyzed using an ACE3 C_{18} column (150 mm × 2.1 mm, particle size

3 µm, ACE) with long RP chromatography [52]. Both methods were set up on a Dionex UltiMate 3000RS UHPLC (ThermoFisher Scientific, Germany) equipped with a quadrupole time-of-flight mass spectrometer (Q-TOF-MS; Bruker, Germany).

Results and Discussion

Electron Tomography and Intracellular Characteristics

Electron tomography analysis of the interdomain biofilm (**Figure 1**) revealed intact and lysed cells from both species *M. cahuitense* (in the segmented tomogram: green) and *D. aggregans* (outer membrane in the segmented tomogram: red). Extracellular vesicles (blue) and bacterial flagella (yellow) were intertwined within the network. The bacterium's complex cell structure is particularly noteworthy: the irregularly formed and therefore enlarged cell surface (red) is separated from the cytoplasmic membrane (pink) by a large periplasm with a width of 25–130 nm (with a mean of 73 nm). On average, the resulting periplasmic volume is about 50% of the total cell volume (range: 20–80%). With that, it exceeds the usual periplasmic space in Gram-negative bacteria which contributes to 20–40% of the total cell volume (estimated from a distance between cytoplasmic and outer membrane of 25–30 nm) [53,54]. The periplasm serves as the cell's checkpoint for quality control [55–57], contains the essential catalyst of the oxidative protein-folding machinery for disulfide bond formation [58], and metabolic enzymes like nitrate reductases and hydrogenases are located in the periplasm [59–61]. In two *Desulfovibrio* species, *D. vulgaris* and *D. gigas*, a [NiFe] hydrogenase, which is involved in both hydrogen uptake and production, is located in the periplasm [62]. An enlarged periplasm was also shown for *D. vulgaris* [63]. In our study, the cytoplasmic membrane of most cells of *D. aggregans* exhibits tubular invaginations into the cytoplasm. This shows that in *D. aggregans* the surface area of the bacterial cytoplasmic membrane is highly enlarged, probably hosting several membrane proteins (e.g. transporters or redox complexes). In addition, the electron tomograms reveal the presence of electron-dense objects in the bacterial cytoplasm, which might hint at storage granules. Similar particles occurred in the archaeal cells. Nile red staining showed that intracellular PHA/PHB storages granules were present in *M. cahuitense* cells but absent in *D. aggregans* when grown in

296 co-culture (data not shown). Direct cell-cell contacts were observed on intra- and interspecies
297 levels.

298 **Spatial Distribution of Cells and EPS within the Biofilm**

299 In this work, we specifically tailored the FISH staining method for analyzing the extremely dense,
300 stable biofilm of this consortium, containing cells with very different cell envelope chemistry and
301 architecture: an archaeal pseudomurein cell wall and a Gram-negative, bacterial cell envelope,
302 with two membranes. The achromopeptidase treatment enhanced deep probe penetration into the
303 EPS and permeability of archaeal cells, while the DOPE probes raised the overall fluorescent
304 signal. **Figure 2a** shows that the distribution of individual cells within the biofilm followed a
305 salient pattern: While methanogenic cells were both planktonic as well as integrated into the
306 biofilm (**Figure 2b**), the bacterial cells almost exclusively appeared within the biofilm matrix
307 (**Figure 2c**). The bacteria were either evenly distributed as individual cells between the
308 methanogens or aggregated into dense cell clumps with a diameter of up to 200 µm.
309 The visualization of EPS sugars by CLSM using ConA and IB4 shows that both pure cultures (M
310 and S) are likely to produce certain sugar residues (**Figure 3**). However, the portion of EPS
311 produced by the bacterial partner (S) was considerably higher, when compared to cell numbers.
312 IB4 and ConA stained similar areas within the biofilms. IB4, however, also targeted the cell
313 surfaces of both prokaryotic cells whereas ConA was only found in the EPS. Additionally, ConA
314 not only binds to α-mannopyranosyl and α-glucopyranosyl residues, but non-specific binding was
315 also reported for polysaccharides like alginate, dextran or glycogen [37,64] and sphingans [65].
316 For that reason, the amount of these sugar residues might be overestimated. Nevertheless, the
317 proportion of EPS produced by *D. aggregans* widely surpasses the production in *M. cahuitense*.

EPS Composition and Sugar Quantification

Following the first results on EPS origin and quantity gathered from CLSM analyses, the biofilm was further surveyed regarding eDNA, protein, and polysaccharides within the biofilm suspension (BF), the total extracellular material (TEM), and the extracellular polymeric substance (EPS) components, as well as the monosaccharides detected in the EPS (**Figure *4***). This was done for all four cultures: *M. cahuitense* (M), *D. aggregans* (S), the original consortium (K), and the artificial co-culture (Ka).

As reported for *Sulfolobus acidocaldarius* [41,44], protein and sugar concentrations in BF of the four cultures exceeded those determined for TEM and EPS samples. Due to the permanent biofilm formation in *Desulfomicrobium*, it was not possible to quantify the EPS compounds in fg $cell^{-1}$ as suggested by Jachlewski et al. [41]. Additionally, metal sulfides aggregated into the sulfate reducer's biofilm matrix and contributed to the wet weight of the analyzed sample. This means that the analyzed culture S contained less cell mass than a pure culture of M, which leads to a bias in the data. This was also reflected in the concentrations of all analyzed substances (**Figure *4*a**) which were significantly lower in the S culture compared to M, K, and Ka. The eDNA in S was even completely missing in BF. In the EPS fraction, however, eDNA compared to protein and polysaccharides indicates that the total eDNA is directly linked to TEM and EPS in *Desulfomicrobium*, which explains the repeatedly detected stability of this specific biofilm [17]. Accordingly, eDNA was reported to constitute an integral building element for biofilm stability [66]. The original consortium K showed considerably higher concentrations of eDNA, polysaccharides, and protein in all BF samples, particularly for eDNA, where levels of K exceeded S and M values by 99% and 85%, respectively. Besides this, K and Ka showed very similar concentrations in all analyses. Protein concentrations were, again, lowest for S, similar for M and K, but significantly higher in the artificial consortium Ka in the TEM and EPS fractions. The total polysaccharide concentrations in TEM and EPS were low in both S and M, and highest

for K, followed by Ka. Overall, the content of protein and sugars in TEM and EPS samples were higher for Ka (protein) or both co-cultures K and Ka (polysaccharides).

HPLC analysis of EPS polysaccharides revealed L-rhamnose, D-glucosamine, D-galactose, D-glucose, D-xylose, and D-mannose in all cultures, while D-ribose was lacking in the EPS of the sulfate reducer (**Figure *4*b**). Ribose is most likely derived from eRNA, which was reported to be an integral element of microbial biofilms [67] that can regulate EPS synthesis [68,69] or repress cell motility [70] in Bacteria and Archaea. The highest sugar concentration in the EPS of culture S was detected for glucose (15 µM) and mannose (7 µM). This also corresponds to the ConA staining results previously described. While glucose concentrations in M (5 µM) were considerably lower, glucose concentrations in cultures K and Ka (12–13 µM) were increased due to the presence of S and its impact on the biofilm matrix. Studies in *E. coli* showed that D-mannose is overrepresented in biofilms compared to planktonic cells [71], which emphasizes the effect of the dense bacterial biofilm on EPS composition. Glucosamine and galactose levels were lowest in culture S and xylose levels were similar for all four cultures. All of the detected sugars were previously reported for microbial biofilms [72].

Intra- and Extracellular Metabolites and EPS-Associated Metabolites

Next, we performed a comprehensive comparison of intra- and extracellular as well as EPS-associated metabolites. Interestingly, we found significant metabolic changes between pure cultures and the co-cultures. Formate was detected intracellularly for all cultures, but extracellularly only in the bacterial culture (3 mM) and in lower concentrations in the consortium cultures (0.7–1.5 mM). As *D. aggregans* cannot use formate as a substrate, the methanogenic partner, for which formate usage is confirmed, might metabolize this organic acid produced by the bacterium [17]. Oxaloacetic acid was found intra- and extracellularly in co- and pure cultures of methanogens with concentrations of 0.1–1 mM and 0.05–0.1 mM, respectively, and in the

sulfate reducer's cultures it only occurred extracellularly. Propionate was found extracellularly in the methanogenic cultures, but intracellularly in all four cultures. Propionate is a typical substrate for some sulfate reducers; *Desulfomicrobium aggregans*, however, is not known to be able to utilize it [17].

Biofilm metabolomes are diverse and change over time [73]. Some typical, biofilm-associated metabolites detected in all methanogenic cultures (M, K, Ka) were 2,3-butanediol (0.03–0.05 mM) [74] and amino acids like glutamate, arginine, leucine, and isoleucine (0.008–0.07 mM) [74–76]. Glycine was found in all EPS samples, whereas glutamate, caproate, and myo-inositol only occurred in methanogenic cultures. Caproate was found to be produced when N-acyl-homoserinelactones (AHLs), important autoinductors in bacterial quorum sensing, were released in microbial multispecies communities [77]. In anaerobic sludge, caproate was reported as an inhibitor for acetoclastic methanogens at concentrations as low as 2 mM, however, the inhibition was followed by a community structure shift towards hydrogenotrophic methanogens [78].

Comparative Polar Lipid Analysis

Archaeal lipids, especially those of methanogens, are still sparsely surveyed and thus poorly understood. Therefore, the lipid analyses focused on the detection of archaeal lipids and the identification of changes in lipid composition between pure cultures and consortia. Archaeal lipids present in the methanogenic pure culture and the co-culture were PE-AR, 1G-AR, 2G-AR, deoxy-AR, CL-AR, 1G-GDGT, 2G-GDGT and CL-GDGT (see **Table 1** for details and abbreviations). PS-AR was not detected and PI-AR was only present in the consortium. 1G-AR and CL-AR showed up to eight unsaturated bonds per hydrophobic moiety. Overall, archaeols dominated over GDGTs.

Concerning bacterial lipids, the typical lipids PG-DAG C_{30}–C_{36} and PE-DAG C_{31}–C_{35}, usually found in sulfate reducers [50,79–81], were observed both in S and K. However, other typical lipids of sulfate reducers like DEG, AEG, and PC were absent. PE-DAG-OH occurred in the consortium culture only.

This study reports, for the first time, 1G-AR and CL-AR species with up to 8 unsaturated bonds. Additionally, an extremely rare deoxyhexose archaeol was found in *Methanobacterium* species for the first time. The archaeols PS-AR, PI-AR, and PE-AR are hallmark IPLs of the genus *Methanobacterium* [82] and the last two were observed in *Methanobacterium movilense*, *Methanobacterium oryzae*, and *Methanobacterium lacus* [83]. However, in the present study, PS-AR was neither detected in the methanogenic culture nor in co-culture, while PI-AR only occurred in the co-culture.

The co-culture also contained the bacterial lipid PE-DAG-OH which was not present in the bacterial pure culture nor observed in previous studies of *D. aggregans.* Changes in lipid composition due to environmental changes are common adaptation mechanisms in microorganisms [84]. Such changes in response to hydrogen or nutrient deficiency were reported for *Methanothermobacter thermautotrophicus* [85] and several bacteria [86,87] including fatty acid chain hydroxylations [88].

Conclusions

The structural, chemical, and temporal complexity of EPS was recently summarized with the term 'matrixome' [89]. This term reflects the scope and diverse methodologies implemented to survey interdomain biofilms. The matrixome not only deals with biofilm composition, but includes the analysis of communication and interaction strategies.

As cell-cell contact was established on intra- and interspecies levels for both surveyed strains, it might hint at such interaction like substrate transfer or DIET. For this consortium, DIET might occur via cytochromes on the outer membrane of the sulfate reducer [90] or fimbriae found in the methanogen [17]. Conductive pili were reported for a *Methanobacterium* species from multispecies aggregates, similar to the ones discussed in this study, and DIET from *Desulfovibrio* to *Methanobacterium* is hypothesized [91]. Whether bacterial flagella like those found in *D. aggregans* can support electron transfer, is still controversially discussed [92,93]. Extracellular conductive materials like metal oxides were not present in the biofilm under laboratory conditions but could further contribute to DIET in the natural habitat [94,95]. A second option for electron transfer is indirect interspecies electron transfer (IIET), which refers to the transfer of molecules such as hydrogen or formate [96]. First hints at ample intra- and extracellular metabolic activity in *D. aggregans* are the invaginations of the cytoplasmic membrane, resulting in an enlarged volume of the periplasm, and the presence of extracellular vesicles. The increased production of bacterial lipids in the co-culture might indicate that these are needed for enlarging the cell's capacity for transport or excretion of metabolites, for exporting the precursors of the EPS, and for increasing the number of protein complexes needed in catabolic and anabolic processes [97]. In *M. cahuitense* PHA/PHB storage granules indicate that carbon sources are abundant, while electron donors like hydrogen might be scarce [98]. In general, metabolic adaptations may derive from intraspecies effects of co-cultivation [85–88] or arise from changes in biofilm formation [71]. As the sulfate reducer readily forms a biofilm when cultivated as pure culture, the influence

of planktonic *Desulfomicrobium* cells could not be taken into account Direct substrate transfer is suggested for formate, which is produced by *D. aggregans* (this study) and utilized as a carbon source by *M. cahuitense* [17]. Vice versa, the methanogens produce propionate, which is a typical substrate for many sulfate reducers including *Desulfomicrobium* species. Nevertheless, in pure culture, *D. aggregans* did not utilize it in previous studies. As propionate was only detected intracellularly in the co-culture, this might hint at diauxic growth or a specialized propionate utilization in *D. aggregans* that only occurs when both organisms are grown together. Based on our comprehensive characterization of this biofilm, a hypothetical overview of the metabolic processes and interactions was drafted (**Figure 5**). As indicated by FISH, *D. aggregans* cells occurred in densely packed, monospecies aggregates or were evenly distributed as individual cells within the interdomain biofilm matrix. Whether this indicates that two different cell types with diverse metabolic characteristics occur, remains an open question. In the natural habitat, the organisms grow in macroscopically visible biofilm aggregates attached to the concrete walls of a water-filled, ancient oil well with constant gas bubbles [17]. The biofilm's position close to the oxygen-rich atmosphere, as well as a blackish-greenish color, indicates photosynthetic activity and oxygen influence. In this biotope, the co-culture might not only profit from attachment, but also from the creation of stable conditions, hydrogen availability, and substrate exchange. Another interesting finding is that *D. aggregans* never occurred as individual cells, but always in aggregates under laboratory conditions. As the pond was largely covered with biofilm, this might be an unusual permanent biofilm strategy characteristic for this habitat. As *M. cahuitense* exists both in a planktonic state as well as in the biofilm together with *D. aggregans*, the methanogen might have actively chosen the sulfate reducer as a valuable partner in this ecosystem. Due to the bacterium's production of a dense and firm EPS matrix and the generation of hydrogen sulfide, the biofilm is constantly kept anoxic, which is important for the methanogen to be able to thrive.

The fact that the original biofilm can be re-created artificially by merging the pure cultures emphasizes the ecological importance of the community, as the consortium can separate and reunite depending on environmentally favorable conditions. Such separation and reconstitution capacities have not been reported for other archaeal or archaeal-bacterial communities like *Ignicoccus* and *Nanoarchaeum* [99] or for closely related species like *M. subterraneum* and *D. baculatum* [17].

In summary, the authors suggest that *M. cahuitense* and *D. aggregans* thrive, untypical for methanogens and sulfate reducers, in peaceful, syntrophic co-culture rather than in severe competition for nutrients.

Acknowledgments

We thank the entire team at the International FISH Course at the Division of Microbial Ecology, University of Vienna, Austria, for their dedicated support and troubleshooting. Furthermore, we thank the Costa Rican authorities CONAGEBIO and SINAC-ACLAC-MINAE for their support under permits no. SINAC-ACLAC-PIME-R-030-2016 and R-044-2016-OT-CONAGEBIO. L.K. and B.S. acknowledge funding by the German Research Foundation (DFG SI 642/13-1)

Contributions

DG, HH, and RR designed the study. LD, RR, AK, and AB performed electron microscopy. LD performed FISH and CLSM experiments. BS supported the design and execution of EPS analysis, LK, JM, and LD performed experiments. RT and MA designed and executed HPLC analysis. WH and WG designed the metabolomics analysis, BD, CB, and LD performed experiments. KUH and HH designed the lipid analysis and SC performed experiments. LD, LK, RR, MA, and BD created figures. LD wrote the manuscript and all authors revised the manuscript.

Data Availability Statement

All data generated or analyzed during this study are included in this published article and its supplementary information files.

References

[1] Rajeev L, Luning EG, Altenburg S, Zane GM, Baidoo EEK, Catena M, et al. Identification of a cyclic-di-GMP-modulating response regulator that impacts biofilm formation in a model sulfate reducing bacterium. Front Microbiol 2014;5. https://doi.org/10.3389/fmicb.2014.00382.

[2] Orell A, Tripp V, Aliaga-Tobar V, Albers SV, Maracaja-Coutinho V, Randau L. A regulatory RNA is involved in RNA duplex formation and biofilm regulation in *Sulfolobus acidocaldarius*. Nucleic Acids Res 2018;46:4794–806. https://doi.org/10.1093/nar/gky144.

[3] Koerdt A, Jachlewski S, Ghosh A, Wingender J, Siebers B, Albers S V. Complementation of *Sulfolobus solfataricus* PBL2025 with an α-mannosidase: effects on surface attachment and biofilm formation. Extremophiles 2012;16:115–25. https://doi.org/10.1007/s00792-011-0411-2.

[4] Zolghadr B, Kling A, Koerdt A, Driessen AJM, Rachel R, Albers SV. Appendage-mediated surface adherence of *Sulfolobus solfataricus*. J Bacteriol 2010;192:104–10. https://doi.org/10.1128/JB.01061-09.

[5] Procópio L. Microbially induced corrosion impacts on the oil industry. Arch Microbiol 2022;204:1–6. https://doi.org/10.1007/s00203-022-02755-7.

[6] Flemming HC, Neu TR, Wozniak DJ. The EPS matrix: the “house of biofilm cells.” J Bacteriol 2007;189:7945–7. https://doi.org/10.1128/JB.00858-07.

[7] Panlilio H, Rice C V. The role of extracellular DNA in the formation, architecture, stability, and treatment of bacterial biofilms. Biotechnol Bioeng 2021;118:2129–41. https://doi.org/10.1002/bit.27760.

[8] Schmitt J, Flemming H-C. Water binding in biofilms. Water Science and Technology 1999;39:77–82. https://doi.org/10.1016/S0273-1223(99)00153-5.

[9] Zhang L, Fritsch M, Hammond L, Landreville R, Slatculescu C, Colavita A, et al. Identification of genes involved in *Pseudomonas aeruginosa* biofilm-specific resistance to antibiotics. PLoS One 2013;8. https://doi.org/10.1371/journal.pone.0061625.

[10] Rudolph C, Wanner G, Huber R. Natural communities of novel Archaea and Bacteria growing in cold sulfurous springs with a string-of-pearls-like morphology. Appl Environ Microbiol 2001;67:2336–44. https://doi.org/10.1128/AEM.67.5.2336-2344.2001.

[11] Jahn U, Gallenberger M, Paper W, Junglas B, Eisenreich W, Stetter KO, et al. *Nanoarchaeum equitans* and *Ignicoccus hospitalis*: New insights into a unique, intimate association of two Archaea. J Bacteriol 2008;190:1743–50. https://doi.org/10.1128/JB.01731-07.

[12] Heimerl T, Flechsler J, Pickl C, Heinz V, Salecker B, Zweck J, et al. A complex endomembrane system in the Archaeon *Ignicoccus hospitalis* tapped by *Nanoarchaeum equitans*. Front Microbiol 2017;8. https://doi.org/10.3389/fmicb.2017.01072.

[13] Johnson MD, Shepherd DC, Sakai HD, Mudaliyar M, Pandurangan AP, Short FL, et al. Cell-to-cell interactions revealed by cryo-tomography of a DPANN co-culture system. Nat Commun 2024;15:7066. https://doi.org/10.1038/s41467-024-51159-2.

[14] Hausner M, Wuertz S. High rates of conjugation in bacterial biofilms as determined by quantitative in situ analysis. Appl Environ Microbiol 1999;65:3710–3. https://doi.org/10.1128/AEM.65.8.3710-3713.1999.

[15] Lovley DR. Syntrophy goes electric: direct interspecies electron transfer. Annu Rev Microbiol 2017;71:643–64. https://doi.org/10.1146/annurev-micro-030117.

[16] Egland PG, Palmer RJ, Kolenbrander PE, Kaiser AD. Interspecies communication in *Streptococcus gordonii–Veillonella atypica* biofilms: signaling in flow conditions requires juxtaposition. PNAS 2004;101. https://doi.org/10.1073pnas.0407457101.

[17] Dengler L, Meier J, Klingl A, Nißl L, Bellack A, Grohmann D, et al. A novel interdomain consortium from a Costa Rican oil well composed of *Methanobacterium cahuitense* sp. nov. and *Desulfomicrobium aggregans* sp. nov. Arch Microbiol 2023;205. https://doi.org/10.1007/s00203-023-03533-9.

[18] Kristjansson JK, Schönheit P. Why do sulfate-reducing bacteria outcompete methanogenic bacteria for substrates? Oecologia 1983;60:264–6. https://doi.org/10.1007/BF00379530.

[19] Kristjansson JK, Schönheit P, Thauer RK. Different Ks values for hydrogen of methanogenic bacteria and sulfate reducing bacteria: An explanation for the apparent inhibition of methanogenesis by sulfate. Arch Microbiol 1982;131:278–82. https://doi.org/10.1007/BF00405893.

[20] Plugge CM, Zhang W, Scholten JCM, Stams AJM. Metabolic flexibility of sulfate-reducing bacteria. Front Microbiol 2011;2:1–8. https://doi.org/10.3389/fmicb.2011.00081.

[21] Raskin L, Rittmann BE, Stahl DA. Competition and coexistence of sulfate-reducing and methanogenic populations in anaerobic biofilms. Appl Environ Microbiol 1996;62:3847–57. https://doi.org/10.1128/aem.62.10.3847-3857.1996.

[22] Ozuolmez D, Na H, Lever MA, Kjeldsen KU, Jørgensen BB, Plugge CM. Methanogenic archaea and sulfate reducing bacteria co-cultured on acetate: Teamwork or coexistence? Front Microbiol 2015;6:1–12. https://doi.org/10.3389/fmicb.2015.00492.

[23] Rachel R, Meyer C, Klingl A, Gürster S, Heimerl T, Wasserburger N, et al. Analysis of the ultrastructure of Archaea by electron microscopy. Methods Cell Biol, vol. 96, 2010, p. 47–69. https://doi.org/10.1016/S0091-679X(10)96003-2.

[24] Mastronarde DN. Automated electron microscope tomography using robust prediction of specimen movements. J Struct Biol 2005;152:36–51. https://doi.org/10.1016/j.jsb.2005.07.007.

[25] Rachel R, Walther P, Maaßen C, Daberkow I, Matsuoka M, Witzgall R. Dual-axis STEM tomography at 200 kV: Setup, performance, limitations. J Struct Biol 2020;211:107551. https://doi.org/10.1016/j.jsb.2020.107551.

[26] Kremer JR, Mastronarde DN, McIntosh JR. Computer visualization of three-dimensional image data using IMOD. J Struct Biol 1996;116:71–6. https://doi.org/10.1006/jsbi.1996.0013.

[27] Greenspan P, Mayer EP, Fowler SD. Nile Red: a selective fluorescent stain for intracellular lipid droplets. J Cell Biol 1985;100:965–73. https://doi.org/10.1083/jcb.100.3.965.

[28] Spiekermann P, Rehm BHA, Kalscheuer R, Baumeister D, Steinbüchel A. A sensitive, viable-colony staining method using Nile red for direct screening of bacteria that accumulate polyhydroxyalkanoic acids and other lipid storage compounds. Arch Microbiol 1999;171:73–80. https://doi.org/10.1007/s002030050681.

[29] Daims H, Bruhl A, Amann R, Schleifer K-H, Wagner M. The domain-specific probe EUB338 is insufficient for the detection of all Bacteria: development and evaluation of a more comprehensive probe set. Syst Appl Microbiol 1999;22:434–44. https://doi.org/10.1016/S0723-2020(99)80053-8.

[30] Stoecker K, Dorninger C, Daims H, Wagner M. Double labeling of oligonucleotide probes for fluorescence in situ hybridization (DOPE-FISH) improves signal intensity

and increases rRNA accessibility. Appl Environ Microbiol 2010;76:922–6. https://doi.org/10.1128/AEM.02456-09.

[31] Wendeberg A. Fluorescence in situ hybridization for the identification of environmental microbes. Cold Spring Harb Protoc 2010. https://doi.org/10.1101/pdb.prot5366.

[32] Amann RI, Krumholz L, Stahl DA. Fluorescent-oligonucleotide probing of whole cells for determinative, phylogenetic, and environmental studies in microbiology. J Bacteriol 1990;172:762–70. https://doi.org/10.1128/jb.172.2.762-770.1990.

[33] Amann RI, Binder BJ, Olson RJ, Chisholm SW, Devereux R, Stahl' DA. Combination of 16S rRNA-Targeted oligonucleotide probes with flow cytometry for analyzing mixed microbial populations. Appl Environ Microbiol 1990;56:1919–25. https://doi.org/10.1128/aem.56.6.1919-1925.1990.

[34] Wallner G, Amann R, Beisker W. Optimizing fluorescent in situ hybridization with rRNA-targeted oligonucleotide probes for flow cytometric identification of microorganisms. Cytometry 1993;14:136–43. https://doi.org/10.1002/cyto.990140205.

[35] Sekar R, Pernthaler A, Pernthaler J, Warnecke F, Posch T, Amann R. An improved protocol for quantification of freshwater *Actinobacteria* by fluorescence in situ hybridization. Appl Environ Microbiol 2003;69:2928–35. https://doi.org/10.1128/AEM.69.5.2928-2935.2003.

[36] CARD-FISH hybridization buffer. Cold Spring Harb Protoc 2010;2010. https://doi.org/10.1101/pdb.rec12119.

[37] Strathmann M, Wingender J, Flemming HC. Application of fluorescently labelled lectins for the visualization and biochemical characterization of polysaccharides in biofilms of *Pseudomonas aeruginosa*. J Microbiol Methods 2002;50:237–48. https://doi.org/10.1016/S0167-7012(02)00032-5.

[38] Küper U, Meyer C, Müller V, Rachel R, Huber H. Energized outer membrane and spatial separation of metabolic processes in the hyperthermophilic Archaeon *Ignicoccus hospitalis*. Proc Natl Acad Sci U S A 2010;107:3152–6. https://doi.org/10.1073/pnas.0911711107.

[39] Kiernan JA. Strategies for preventing detachment of sections from glass slides. Micros Today 1999;7:20–4. https://doi.org/10.1017/s1551929500064622.

[40] Schneider CA, Rasband WS, Eliceiri KW. NIH Image to ImageJ: 25 years of image analysis. Nat Methods 2012;9:671–5. https://doi.org/10.1038/nmeth.2089.

[41] Jachlewski S, Jachlewski WD, Linne U, Bräsen C, Wingender J, Siebers B. Isolation of extracellular polymeric substances from biofilms of the thermoacidophilic archaeon *Sulfolobus acidocaldarius*. Front Bioeng Biotechnol 2015;3:1–11. https://doi.org/10.3389/fbioe.2015.00123.

[42] Peterson GL. Review of the folin phenol protein quantitation method of Lowry, Rosebrough, Farr and Randall. Anal Biochem 1979;100:201–20. https://doi.org/10.1016/0003-2697(79)90222-7.

[43] Dubois Michel, Gilles KA, Hamilton JK, Rebers PA, Smith Fred. Colorimetric method for determination of sugars and related substances. Anal Chem 1956;28:350–6. https://doi.org/10.1021/ac60111a017.

[44] Kuschmierz L, Meyer M, Bräsen C, Wingender J, Schmitz OJ, Siebers B. Exopolysaccharide composition and size in *Sulfolobus acidocaldarius* biofilms. Front Microbiol 2022;13. https://doi.org/10.3389/fmicb.2022.982745.

[45] Reboul R, Geserick C, Pabst M, Frey B, Wittmann D, Lütz-Meindl U, et al. Down-regulation of UDP-glucuronic acid biosynthesis leads to swollen plant cell walls and severe developmental defects associated with changes in pectic polysaccharides. Journal of Biological Chemistry 2011;286:39982–92. https://doi.org/10.1074/jbc.M111.255695.

[46] Gronwald W, Klein MS, Kaspar H, Fagerer SR, Nürnberger N, Dettmer K, et al. Urinary Metabolite Quantification Employing 2D NMR Spectroscopy. Anal Chem 2008;80:9288–97. https://doi.org/10.1021/ac801627c.

[47] R Core Team. R: A Language and Environment for Statistical Computing. R Foundation for Statistical Computing 2023. https://www.R-project.org/ (accessed August 24, 2024).

[48] Huber W, Von Heydebreck A, Sültmann H, Poustka A, Vingron M. Variance stabilization applied to microarray data calibration and to the quantification of differential expression. Bioinformatics, vol. 18, Oxford University Press; 2002. https://doi.org/10.1093/bioinformatics/18.suppl_1.S96.

[49] Bligh EG, Dyer WJ. A rapid method of total lipid extraction and purification. Can J Biochem Physiol 1959;37:911–7. https://doi.org/10.1139/o59-099.

[50] Sturt HF, Summons RE, Smith K, Elvert M, Hinrichs K. Intact polar membrane lipids in prokaryotes and sediments deciphered by high-performance liquid chromatography/electrospray ionization multistage mass spectrometry—new biomarkers for biogeochemistry and microbial ecology. Rapid Communications in Mass Spectrometry 2004;18:617–28. https://doi.org/10.1002/rcm.1378.

[51] Wörmer L, Lipp JS, Schröder JM, Hinrichs KU. Application of two new LC-ESI-MS methods for improved detection of intact polar lipids (IPLs) in environmental samples. Org Geochem 2013;59:10–21. https://doi.org/10.1016/j.orggeochem.2013.03.004.

[52] Zhu C, Lipp JS, Wörmer L, Becker KW, Schröder J, Hinrichs KU. Comprehensive glycerol ether lipid fingerprints through a novel reversed phase liquid chromatography-mass spectrometry protocol. Org Geochem 2013;65:53–62. https://doi.org/10.1016/j.orggeochem.2013.09.012.

[53] Van Wielink JE, Duine JA. How big is the periplasmic space? vol. 155. Kluwer Academic Publishers; 1990.

[54] Stock JB, Rauch B, Roseman S. Periplasmic space in *Salmonella typhimurium* and *Escherichia coli*. J Biol Chem 1977;252. https://doi.org/10.1016/S0021-9258(17)41044-1.

[55] Merdanovic M, Clausen T, Kaiser M, Huber R, Ehrmann M. Protein quality control in the bacterial periplasm. Annu Rev Microbiol 2011;65:149–68. https://doi.org/10.1146/annurev-micro-090110-102925.

[56] Duguay AR, Silhavy TJ. Quality control in the bacterial periplasm. Biochim Biophys Acta 2004;1694:121–34. https://doi.org/10.1016/j.bbamcr.2004.04.012.

[57] Miot M, Betton J-M. Protein quality control in the bacterial periplasm. Microb Cell Fact 2004;3. https://doi.org/10.1186/1475-2859-3-4.

[58] Bardwell JCA, Lee J-O, Jander G, Martin N, Belint D, Beckwith J. A pathway for disulfide bond formation *in vivo*. Proceedings of the National Academy of Sciences 1993;90:1038–42. https://doi.org/10.1073/pnas.90.3.1038.

[59] Stewart V, Lu Y, Darwin AJ. Periplasmic nitrate reductase (NapABC enzyme) supports anaerobic respiration by *Escherichia coli* K-12. J Bacteriol 2002;184:1314–23. https://doi.org/10.1128/JB.184.5.1314-1323.2002.

[60] Potter L, Angove H, Richardson D, Cole J. Nitrate reduction in the periplasm of gram-negative bacteria. Adv Microb Physiol 2001;45:51–112. https://doi.org/10.1016/S0065-2911(01)45002-8.

[61] Caffrey SM, Park HS, Voordouw JK, He Z, Zhou J, Voordouw G. Function of periplasmic hydrogenases in the sulfate-reducing bacterium *Desulfovibrio vulgaris* Hildenborough. J Bacteriol 2007;189:6159–67. https://doi.org/10.1128/JB.00747-07.

[62] Hatchikian EC, Forget N, Bernadac; A., Alazard D, Ollivier B. Involvement of a single periplasmic hydrogenase for both hydrogen uptake and production in some

Desulfovibrio species. Res Microbiol 1995;146:129–41. https://doi.org/10.1016/0923-2508(96)80891-6.

[63] Karnachuk O V., Beletsky A V., Rakitin AL, Ikkert OP, Avakyan MR, Zyusman VS, et al. Antibiotic-resistant *Desulfovibrio* produces H_2S from supplements for animal farming. Microorganisms 2023;11. https://doi.org/10.3390/microorganisms11040838.

[64] Goldstein I J, Hollerman CE, Merrick JM. The interaction of polysaccharides with Concanavalin A. Biochim Biophys Acta 1965;97:68–76. https://doi.org/10.1016/0304-4165(65)90270-9.

[65] Johnsen AR, Hausner M, Schnell A, Wuertz S. Evaluation of fluorescently labeled lectins for noninvasive localization of extracellular polymeric substances in *Sphingomonas* biofilms. Appl Environ Microbiol 2000;66:3487–91. https://doi.org/10.1128/AEM.66.8.3487-3491.2000.

[66] Yang Y, Li M, Zheng X, Ma H, Nerenberg R, Chai H. Extracellular DNA plays a key role in the structural stability of sulfide-based denitrifying biofilms. Science of the Total Environment 2022;838. https://doi.org/10.1016/j.scitotenv.2022.155822.

[67] Mugunthan S, Wong LL, Winnerdy FR, Summers S, Bin Ismail MH, Foo YH, et al. RNA is a key component of extracellular DNA networks in *Pseudomonas aeruginosa* biofilms. Nat Commun 2023;14. https://doi.org/10.1038/s41467-023-43533-3.

[68] Yin L, Zhu W, Chen D, Zhou Y, Lin H. Small noncoding RNA sRNA0426 is involved in regulating biofilm formation in *Streptococcus mutans*. Microbiologyopen 2020;9. https://doi.org/10.1002/mbo3.1096.

[69] Liu MY, Gui G, Wei B, Preston JF, Oakford L, Yüksel Ü, et al. The RNA molecule CsrB binds to the global regulatory protein CsrA and antagonizes its activity in *Escherichia coli*. Journal of Biological Chemistry 1997;272:17502–10. https://doi.org/10.1074/jbc.272.28.17502.

[70] Weilbacher T, Suzuki K, Dubey AK, Wang X, Gudapaty S, Morozov I, et al. A novel sRNA component of the carbon storage regulatory system of *Escherichia coli*. Mol Microbiol 2003;48:657–70. https://doi.org/10.1046/j.1365-2958.2003.03459.x.

[71] Lu H, Que Y, Wu X, Guan T, Guo H. Metabolomics deciphered metabolic reprogramming required for biofilm formation. Sci Rep 2019;9. https://doi.org/10.1038/s41598-019-49603-1.

[72] Jiao Y, Cody GD, Harding AK, Wilmes P, Schrenk M, Wheeler KE, et al. Characterization of extracellular polymeric substances from acidophilic microbial biofilms. Appl Environ Microbiol 2010;76:2916–22. https://doi.org/10.1128/AEM.02289-09.

[73] Malviya J, Alameri AA, Al-Janabi SS, Fawzi OF, Azzawi AL, Obaid RF, et al. Metabolomic profiling of bacterial biofilm: trends, challenges, and an emerging antibiofilm target. World J Microbiol Biotechnol 2023;39. https://doi.org/10.1007/s11274-023-03651-y.

[74] Feliks Junka A, Deja S, Smutnicka D, Szymczyk P, Ziółkowski G, Bartoszewicz M, et al. Differences in metabolic profiles of planktonic and biofilm cells in *Staphylococcus aureus*-1H Nuclear Magnetic Resonance search for candidate biomarkers. Acta Biochim Pol 2013;60:701–6.

[75] Xu Z, Fang X, Wood TK, Huang ZJ. A systems-level approach for investigating *Pseudomonas aeruginosa* biofilm formation. PLoS One 2013;8. https://doi.org/10.1371/journal.pone.0057050.

[76] Yeom J, Shin JH, Yang JY, Kim J, Hwang GS. ^{1}H NMR-based metabolite profiling of planktonic and biofilm cells in *Acinetobacter baumannii* 1656-2. PLoS One 2013;8. https://doi.org/10.1371/journal.pone.0057730.

[77] Li J, Liu H, Wu P, Ding P, Zhang J, Zhang C, et al. Quorum sensing signals enhanced caproate production by changing microbial community in chain elongation enrichments. J Environ Chem Eng 2021;9. https://doi.org/10.1016/j.jece.2021.106623.

[78] Li Z, Qiu S, Xu J, Ge S. Effect of undissociated *n* -caproic acid on methanogen activity and subsequent recovery: methane anabolism and community structure. ACS ES&T Engineering 2024;4:706–16. https://doi.org/10.1021/acsestengg.3c00393.

[79] Rütters H, Sass H, Cypionka H, Rullkötter J. Monoalkylether phospholipids in the sulfate-reducing bacteria Desulfosarcina variabilis and Desulforhabdus amnigenus. Arch Microbiol 2001;176:435–42. https://doi.org/10.1007/s002030100343.

[80] Schubotz F, Lipp JS, Elvert M, Hinrichs KU. Stable carbon isotopic compositions of intact polar lipids reveal complex carbon flow patterns among hydrocarbon degrading microbial communities at the Chapopote asphalt volcano. Geochim Cosmochim Acta 2011;75:4399–415. https://doi.org/10.1016/j.gca.2011.05.018.

[81] Makula RA, Finnerty WR. Phospholipid composition of *Desulfovibrio* species. Journal of Bacterioloy 1974;120:1279–83. https://doi.org/10.1128/jb.120.3.1279-1283.1974.

[82] Koga Y, Nakano M. A dendrogram of archaea based on lipid component parts composition and its relationship to rRNA phylogeny. Syst Appl Microbiol 2008;31:169–82. https://doi.org/10.1016/j.syapm.2008.02.005.

[83] Schirmack J, Mangelsdorf K, Ganzert L, Sand W, Hillebrand-Voiculescu A, Wagner D. *Methanobacterium movilense* sp. nov., a hydrogenotrophic, secondary-alcohol-utilizing methanogen from the anoxic sediment of a subsurface lake. Int J Syst Evol Microbiol 2014;64:522–7. https://doi.org/10.1099/ijs.0.057224-0.

[84] Taubner R-S, Baumann LMF, Steiner M, Pfeifer K, Reischl B, Korynt K, et al. Lipidomics and comparative metabolite excretion analysis of methanogenic archaea

748 reveal organism-specific adaptations to varying temperatures and substrate
749 concentrations. MSystems 2023;8. https://doi.org/10.1128/msystems.01159-22.
750 [85] Yoshinaga MY, Gagen EJ, Wörmer L, Broda NK, Meador TB, Wendt J, et al.
751 *Methanothermobacter thermautotrophicus* modulates its membrane lipids in response to
752 hydrogen and nutrient availability. Front Microbiol 2015;6.
753 https://doi.org/10.3389/fmicb.2015.00005.
754 [86] Ding S, Henkel J V, Hopmans EC, Bale NJ, Koenen M, Villanueva L, et al. Changes in
755 the membrane lipid composition of a *Sulfurimonas* species depend on the electron
756 acceptor used for sulfur oxidation. ISME Communications 2022;2.
757 https://doi.org/10.1038/s43705-022-00207-3.
758 [87] Sohlenkamp C, Geiger O. Bacterial membrane lipids: diversity in structures and
759 pathways. FEMS Microbiol Rev 2015;40:133–59.
760 https://doi.org/10.1093/femsre/fuv008.
761 [88] Huffer S, Clark ME, Ning JC, Blanch HW, Clark DS. Role of alcohols in growth, lipid
762 composition, and membrane fluidity of yeasts, bacteria, and archaea. Appl Environ
763 Microbiol 2011;77:6400–8. https://doi.org/10.1128/AEM.00694-11.
764 [89] Karygianni L, Ren Z, Koo H, Thurnheer T. Biofilm matrixome: extracellular
765 components in structured microbial communities. Trends Microbiol 2020;28:668–81.
766 https://doi.org/10.1016/j.tim.2020.03.016.
767 [90] Lovley DR. Happy together: microbial communities that hook up to swap electrons.
768 ISME Journal 2017;11:327–36. https://doi.org/10.1038/ismej.2016.136.
769 [91] Zheng S, Li M, Liu Y, Liu F. *Desulfovibrio* feeding *Methanobacterium* with electrons in
770 conductive methanogenic aggregates from coastal zones. Water Res 2021;202.
771 https://doi.org/10.1016/j.watres.2021.117490.

[92] Liu X, Zhuo S, Jing X, Yuan Y, Rensing C, Zhou S. Flagella act as *Geobacter* biofilm scaffolds to stabilize biofilm and facilitate extracellular electron transfer. Biosens Bioelectron 2019;146. https://doi.org/10.1016/j.bios.2019.111748.

[93] Sure S, Ackland ML, Torriero AAJ, Adholeya A, Kochar M. Microbial nanowires: an electrifying tale. Microbiology (N Y) 2016;162:2017–28. https://doi.org/10.1099/mic.0.000382.

[94] Dang Y, Sun D, Woodard TL, Wang LY, Nevin KP, Holmes DE. Stimulation of the anaerobic digestion of the dry organic fraction of municipal solid waste (OFMSW) with carbon-based conductive materials. Bioresour Technol 2017;238:30–8. https://doi.org/10.1016/j.biortech.2017.04.021.

[95] Zheng S, Liu F, Li M, Xiao L, Wang O. Comparative transcriptomic insights into the mechanisms of electron transfer in *Geobacter* co-cultures with activated carbon and magnetite. Sci China Life Sci 2018;61:787–98. https://doi.org/10.1007/s11427-017-9177-1.

[96] Schink B, Montag D, Keller A, Müller N. Hydrogen or formate: Alternative key players in methanogenic degradation. Environ Microbiol Rep 2017;9:189–202. https://doi.org/10.1111/1758-2229.12524.

[97] Toyofuku M, Schild S, Kaparakis-Liaskos M, Eberl L. Composition and functions of bacterial membrane vesicles. Nat Rev Microbiol 2023;21:415–30. https://doi.org/10.1038/s41579-023-00875-5.

[98] Shively JM, Cannon GC, Heinhorst S, Bryant DA, DasSarma S, Bazylinski D, et al. Bacterial and Archaeal Inclusions. Encyclopedia of Life Sciences, Wiley; 2011. https://doi.org/10.1002/9780470015902.a0000302.pub3.

[99] Paper W, Jahn U, Hohn MJ, Kronner M, Näther DJ, Burghardt T, et al. *Ignicoccus hospitalis* sp. nov., the host of *Nanoarchaeum equitans*. Int J Syst Evol Microbiol 2007;57:803–8. https://doi.org/10.1099/ijs.0.64721-0.

Tables

Table 1. Archaeal and bacterial lipids detected in the pure cultures (M, S) and the co-culture (K).

		M	K	Reference
Archaeal Lipids	**PE-AR**	+	+	[50,82,83,85]
	PS-AR	–	–	[82,85]
	PI-AR	–	+	[82,83,85]
	1G-AR	+	+	[83]
	2G-AR	+	+	
	deoxy-AR	+	+	
	CL-AR	+	+	
	1G-GDGT	+	+	
	2G-GDGT	+	+	
	CL-GDGT	+	+	
		S	**K**	**Reference**
Bacterial Lipids	**PE-DAG**	+	+	[50,80,81]
	PG-DAG	+	+	[80,81]
	PE-DAG-OH	–	+	
	DEG	–	–	
	AEG	–	–	
	PC	–	–	

+, present; –, absent;

PE, phosphatidyl ethanolamine; PS, phosphatidyl serine; PI, phosphatidyl inositol; PG, phosphatidyl glycerol; AR, archaeol; 1G/2G, mono-/diglycosidic; deoxy; deoxyhexose; CL, core lipid; GDGT, glycerol dialkyl glycerol tetraether; DAG; diacylglycerol; DEG, diether glycerol; AEG, acyl ether glycerol.

Figure Legends

Figure 1. (**a, b)** Selected slices (2.7 nm thick; about 100 nm apart) of a tomogram of the interdomain biofilm comprised of *Methanobacterium cahuitense* and *Desulfomicrobium aggregans*. (**c**) Tomogram segmentation and visualization. Green: *M. cahuitense*; red: *D. aggregans* outer membrane; pink: *D. aggregans* cytoplasmic membrane; yellow: *D. aggregans* flagellum; blue (arrows): vesicles. Bar, 500 nm. 41

Figure 2. Combined DOPE (double labeling of oligonucleotide probes) and[29,30] CARD (catalyzed reporter deposition) Fluorescence in situ hybridization of the co-culture visualized with CLSM (confocal laser scanning microscopy). The merged image displays the interdomain biofilm (**a**) treated with the Oregon Green doubly-labeled archaeal probe Arch915 for methanogenic cells (green) (**b**) and the Cy5 doubly-labeled bacterial probe EUB388 for the sulfate reducer (red) (**c**). NON-EUB was used as a nonsense probe. Bars, 50 µm. 42

Figure 3. CLSM images reporting on the fluorescence of the lectins ConA that binds to α-mannopyranosyl and α-glucopyranosyl residues (green; **b, e**) and IB4 that targets α-D-galactosyl (yellow; **c, f**) produced by pure cultures of *M. cahuitense* (**a, b, c**) and *D. aggregans* (**d, e, f**), respectively. Counterstaining of the microbial cells was performed using DAPI (blue; **a, d**). Bar, 10 µm..... 43

Figure 4. (a) Quantification of eDNA, protein and total sugars for the biofilm suspension (BF), the total extracellular material (TEM), and the extracellular polymeric substance (EPS). (**b**) Identification and quantification of selected EPS sugars by HPLC. Red: *D. aggregans* (S); green: *M. cahuitense* (M); blue: the original co-culture (K); violet: artificial co-culture (Ka). Error bars: standard deviation; N=3..... 44

Figure 5. Hypothetic metabolic processes in the co-culture. The origins of the metabolites are either *M. cahuitense* (green), *D. aggregans* (red), or both organisms (black). Especially,

Figures

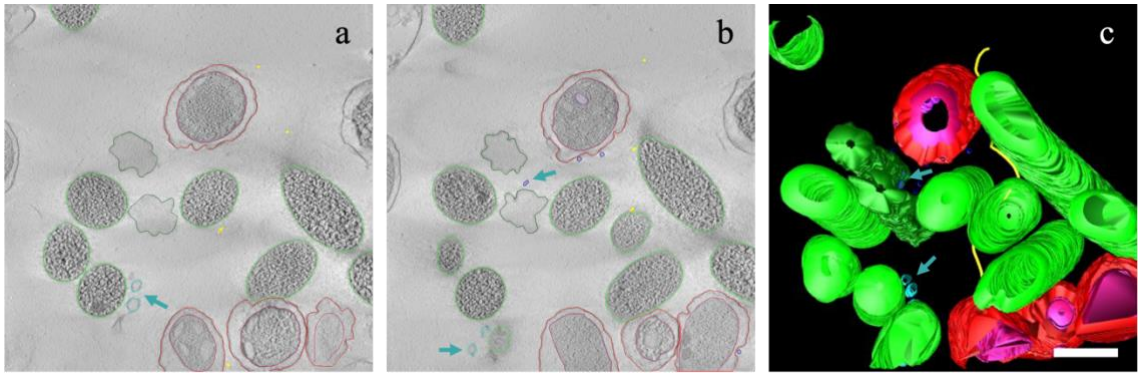

Figure 1. (**a, b)** Selected slices (2.7 nm thick; about 100 nm apart) of a tomogram of the interdomain biofilm comprised of *Methanobacterium cahuitense* and *Desulfomicrobium aggregans*. (**c**) Tomogram segmentation and visualization. Green: *M. cahuitense*; red: *D. aggregans* outer membrane; pink: *D. aggregans* cytoplasmic membrane; yellow: *D. aggregans* flagellum; blue (arrows): vesicles. Bar, 500 nm.

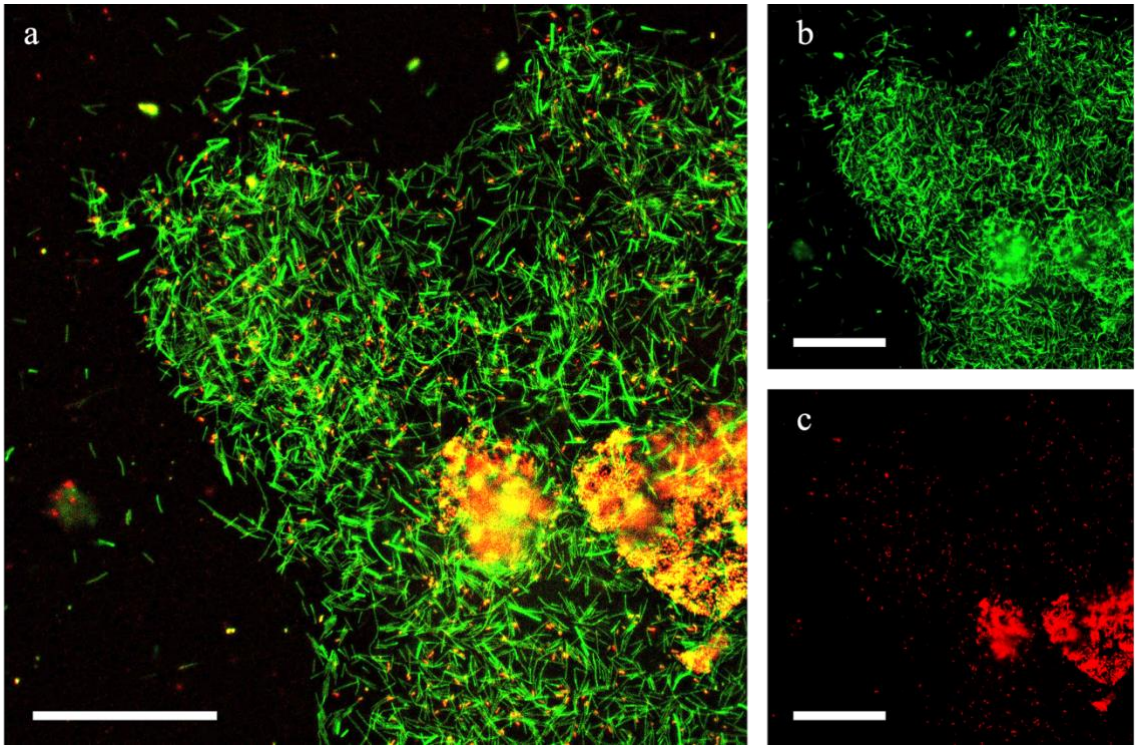

Figure 2. Combined DOPE (double labeling of oligonucleotide probes) and[29,30] CARD (catalyzed reporter deposition) Fluorescence in situ hybridization of the co-culture visualized with CLSM (confocal laser scanning microscopy). The merged image displays the interdomain biofilm (**a**) treated with the Oregon Green doubly-labeled archaeal probe Arch915 for methanogenic cells (green) (**b**) and the Cy5 doubly-labeled bacterial probe EUB388 for the sulfate reducer (red) (**c**). NON-EUB was used as a nonsense probe. Bars, 50 µm.

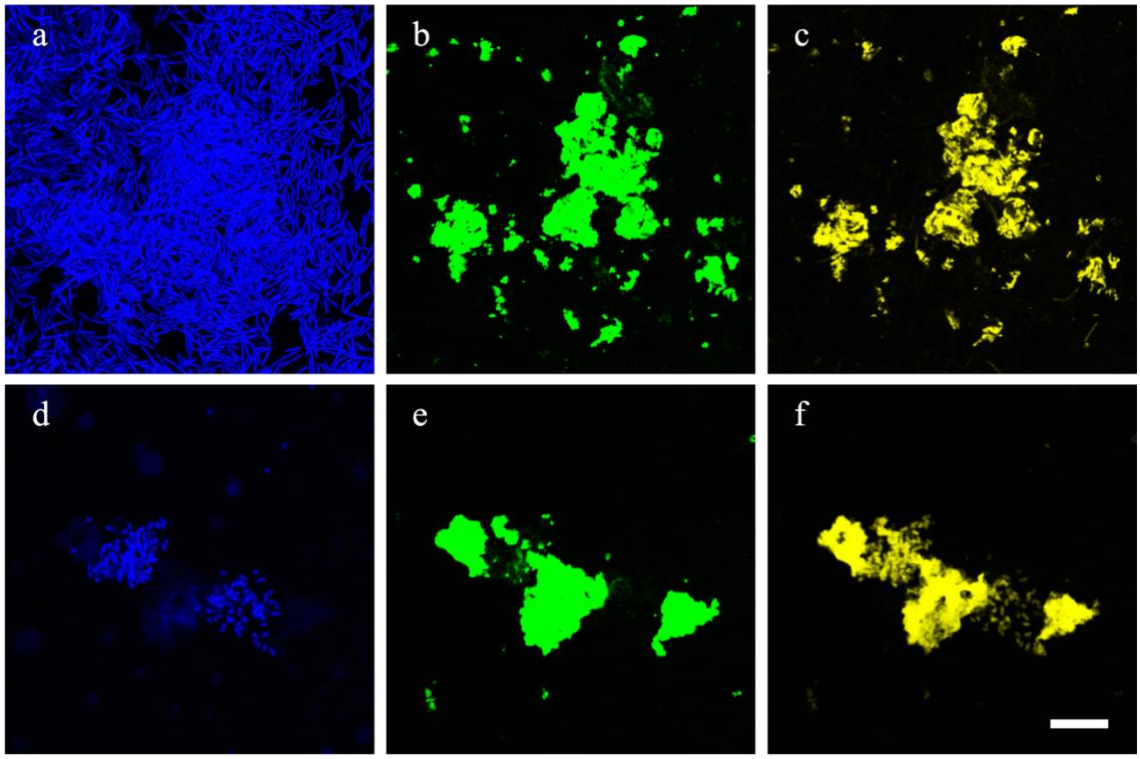

Figure 3. CLSM images reporting on the fluorescence of the lectins ConA that binds to α-mannopyranosyl and α-glucopyranosyl residues (green; **b, e**) and IB4 that targets α-D-galactosyl (yellow; **c, f**) produced by pure cultures of *M. cahuitense* (**a, b, c**) and *D. aggregans* (**d, e, f**), respectively. Counterstaining of the microbial cells was performed using DAPI (blue; **a, d**). Bar, 10 µm.

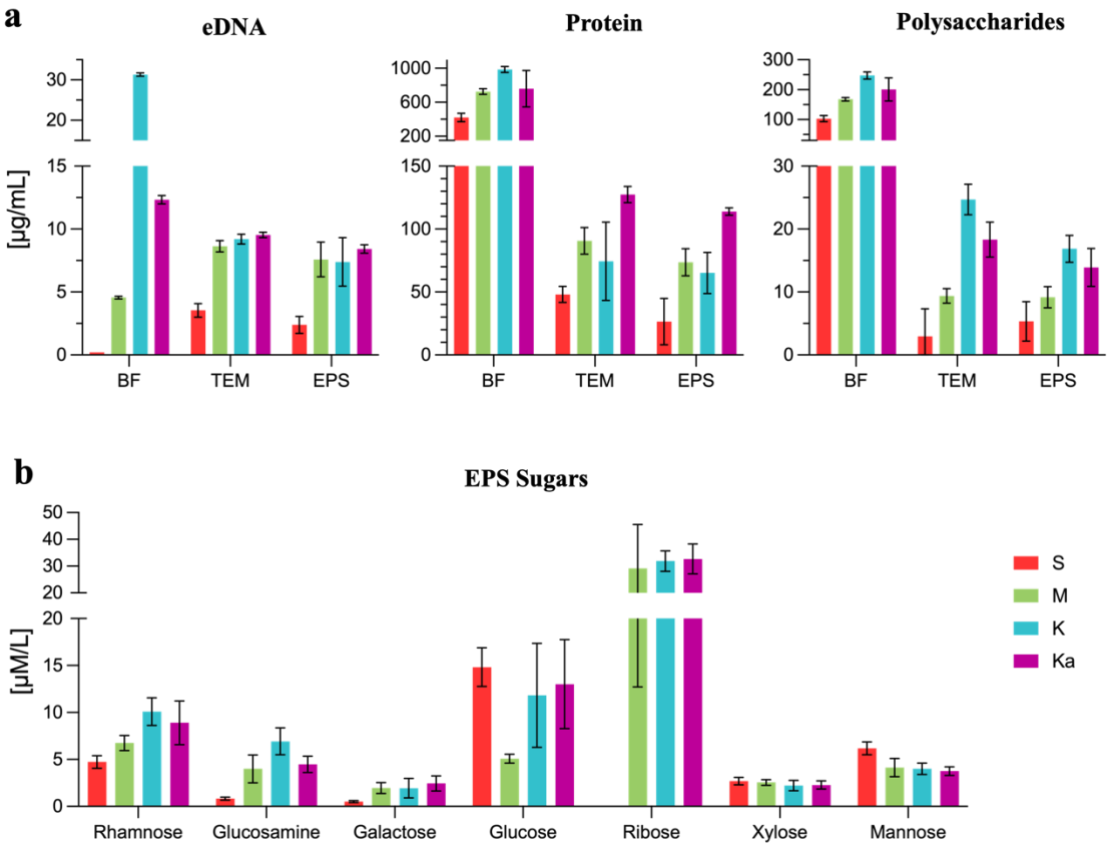

Figure 4. (a) Quantification of eDNA, protein and total sugars for the biofilm suspension (BF), the total extracellular material (TEM), and the extracellular polymeric substance (EPS). (**b**) Identification and quantification of selected EPS sugars by HPLC. Red: *D. aggregans* (S); green: *M. cahuitense* (M); blue: the original co-culture (K); violet: artificial co-culture (Ka). Error bars: standard deviation; N=3.

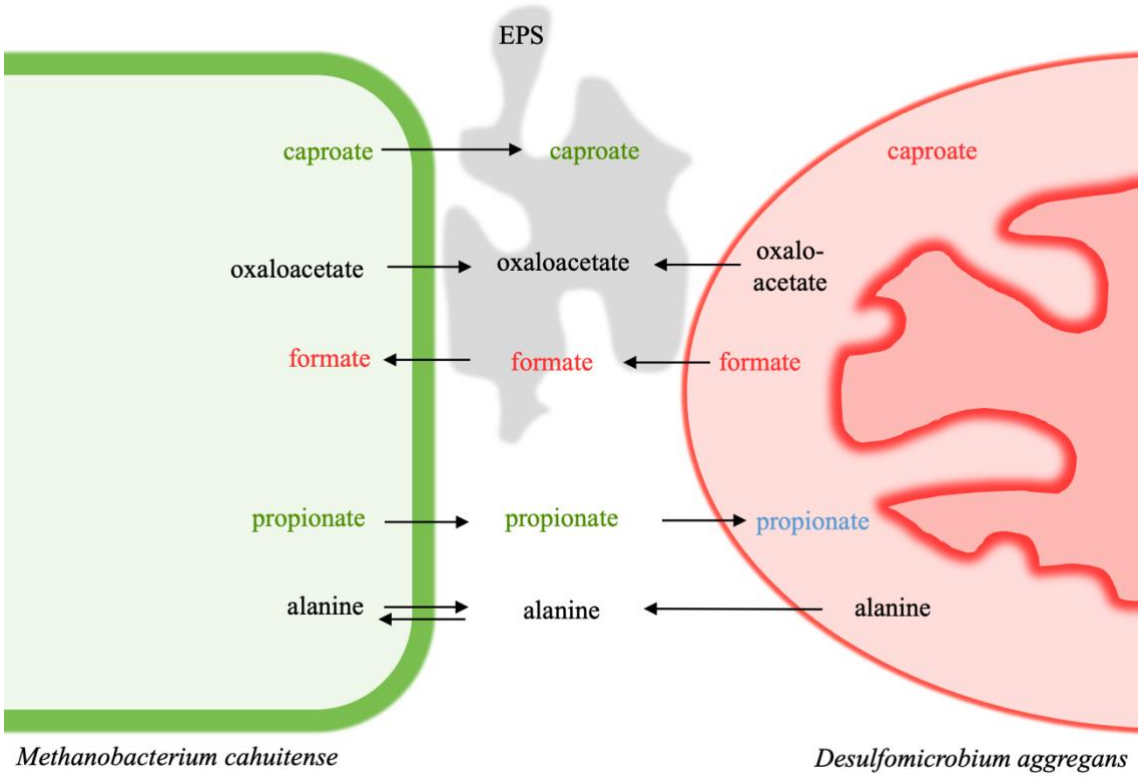

856

857 **Figure 5.** Hypothetic metabolic processes in the co-culture. The origins of the metabolites are either *M. cahuitense*
858 (green), *D. aggregans* (red), or both organisms (black). Especially, caproate, oxaloacetate, and formate were found in
859 the EPS matrix. The hypothetic propionate uptake by *D. aggregans* only occurs when grown in co-culture (blue).

860

Supplementary Material

For supplementary information, please see the separate supplementary material files.